

## **FORCED VIBRATION RESPONSE OF NONLINEAR TOP-LOADED CORRUGATED FIBERBOARD CONTAINERS<sup>1</sup>**

**Thomas J. Urbanik**  
**U.S. Department of Agriculture, Forest Service**  
**Forest Products Laboratory<sup>2</sup>**  
**Madison, Wisconsin 53705-2398**

A nonlinear theory of forced vibration response is developed and applied to corrugated fiberboard containers loaded in top-to-bottom cyclic compression. The theory incorporates an exact undamped free vibration solution and an approximate forced vibration solution for predicting transmissibility curves from empirical nonlinear stiffness and damping functions. The container response at arbitrary precompression load levels and harmonic forcing accelerations is shown to depend on material stiffness, damping, and the respective rates of load-dependent change. Physical constants characterizing various container designs are determined by matching theoretical softening system transmissibility curves to data acquired using a force plate excitation–response system. Results from an experimental study describe the stiffness and damping properties resulting from flute construction, container size, and interior end-pad design characteristics. Favorable or detrimental response characteristics of container stacks can be inferred from the nonlinear material properties of individual containers and the property interactions.

### **INTRODUCTION**

Products in corrugated containers are often shipped in pallet loads or stacking arrangements where top-to-bottom container stiffness determines the likelihood of transportation-induced shock and vibration damage. Cushioning material, product resilience, or the compliance of interior packaging can interact with the container and shift the vibration response between favorable and detrimental conditions. Knowing how to characterize an individual container to predict the response of a whole stack has important implications for designing containers and for assessing safe stacking patterns. A general understanding of vibration protection based on fiber product material can make corrugated fiberboard the material of choice within the packaging and distribution industries.

Standard vibration test methods [1,2] for simulating over-the-road packaging performance can determine primarily the resonant frequencies of a container or stack, but such methods do not fully address how to improve the container. More objective test methods and analysis procedures are needed by which individual containers and their interior components can be evaluated and designed according to criteria that optimize stack dynamic performance. A critical difficulty to overcome in characterizing the container is that corrugated containers follow nonlinear restoring force–deformation characteristics and dissipative force–velocity characteristics. Exact solutions for analyzing the forced vibration response of such systems are virtually nonexistent [3]. Various approximation methods have been applied to analyzing nonlinear systems—each method has unique advantages and restrictions, depending on the characterizations of material stiffness and damping.

---

<sup>1</sup> Funded by USDA Grant No. 85–FSTY–9–0113.

<sup>2</sup> The Forest Products Laboratory is maintained in cooperation with the University of Wisconsin. This article was written and prepared by U.S. Government employees on official time, and it is therefore in the public domain and not subject to copyright.

One of the earliest studies that demonstrated the scope of the problem was that by Godshall [4], who tested and analyzed a specific corrugated container as a spring component in a single-degree-of-freedom (SDOF) system. His frequency response analysis summarized nonlinear stiffness and damping properties with a table of equivalent linear properties, each pair associated with a different experimental combination of static equilibrium top-load and forcing-vibration amplitude. Similar nonlinear behavior, along with the problems of reducing the data, was exhibited when Godshall [5] later evaluated the response of corrugated pads.

Motivated by a need to reduce transportation damage to produce, Peleg proposed a forced vibration model having linear plus cubic stiffness and viscous plus friction damping as a general model for approximating the shock and vibration response of nonlinear cushioned items [6] and unit loads [7]. Physical constants in the model are determined by analyzing dynamic force–deflection hysteresis loops, rather than by analyzing response–frequency curves. The linear plus cubic stiffness function yields an odd function curve symmetric about the origin, with applications to determining an average solution to the equations of motion. Unfortunately, Peleg’s analysis is not easily applied to corrugated containers in a stack where individual containers of equal initial stiffness are subjected to an incrementally increasing static precompression.

In previous research [8], I analyzed the dynamic reaction force beneath a box stack modeled as a linear multiple-degree-of-freedom (MDOF) system. Permanent deformation around the horizontal score line and load sharing with the interior package were found to cause higher corrugated container stiffness with increasing precompression. Boxes at the bottom of a stack became stiffer than those at the top. The model incorporated static load dependent stiffness properties but predicted only an assumed linear behavior based on these properties remaining constant. Knowing how to characterize the dependence of these properties on vibration amplitude could have improved the predictions.

Two important phenomena were found to be associated with corrugated container stiffness: (a) stack vibration response at resonance theoretically decreases with an increasing rate of stiffness change in progressing from the top to bottom tiers, and (b) under conditions where the product does not support the stack weight, cushions softer than the container can theoretically act like vibration absorbers to minimize dynamic loads on the containers, but at the expense of increased product vibration. Using knowledge of favorable container design characteristics that lead to superior stack performance, this report proposes a theory for dealing with experimental vibration data and for determining the nonlinear stiffness and damping properties of individual containers.

## **OBJECTIVE AND SCOPE**

The objective of this report is to propose a nonlinear vibration theory for characterizing corrugated fiber-board containers in terms of parameters known to relate to the dynamic vertical response of MDOF stacks during transportation. We review the concepts for characterizing the response of linear systems subjected to a harmonic base disturbance and introduce equations for predicting top-to-bottom stiffness and damping as functions of load under static conditions. Using the stiffness–load relationship, we predict the undamped cyclic load–deformation curve and the corresponding strain–energy relationship specific to corrugated containers.

The section Free Vibration Response describes how to determine the undamped natural frequency of our nonlinear system. Starting with other force–deformation and elastic energy relationships, the method can have applications to general nonlinear systems. The solution given is an exact solution in the sense that the numerical solutions proposed can be carried out to any degree of accuracy. Vibration amplitude is characterized in terms of the maximum response velocity, as a way of dealing with a nonharmonic system response.

In the section Forced Vibration Response, we propose an approximate solution to calculating nonlinear system transmissibility curves. Expressions for linearized stiffness and damping are determined from the average deformation during free vibration. We assume that expressions for nonlinear natural frequency and ratio of critical

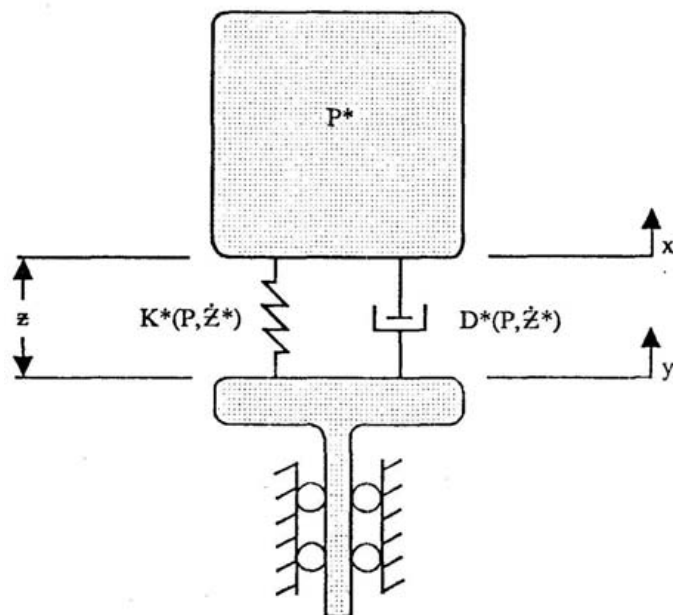


Fig. 1—Representation of a *SDOF* spring–mass system. Properties of stiffness  $K^*$  and damping  $D^*$  depend on the static equilibrium deformation at load  $P$  and on the undamped free vibration velocity amplitude  $\dot{Z}^*$  of the equivalent guided system having an average generalized weight  $P^*$ .

damping can be substituted into the linear transmissibility relationship to predict the response of an equivalent linear system at each relative response velocity.

Experiments are described under a factorial design for characterizing the response of corrugated containers using the proposed theory. The experimental procedure can be applied to individual containers, their interior cushioning, and container stacks. By fitting nonlinear transmissibility curves to data, we evaluate a set of containers in terms of design characteristics known to relate to the dynamic response of container stacks.

## THEORY

### Basic Linear Theory

The motion of the SDOF system mass of static weight  $P$  in Figure 1 is described by the second order ordinary differential equation

$$K(y - x) + D\left(\frac{dy}{dt} - \frac{dx}{dt}\right) = \frac{P^*}{g} \frac{d^2x}{dt^2} \quad (1)$$

where  $K$  is stiffness,  $y$  and  $x$  are disturbance and response displacement, respectively,  $D$  is damping,  $t$  time,  $P^*$  generalized dynamic weight, and  $g$  gravitational acceleration. The equation is expressed in terms of weight instead of mass to agree with nomenclature that accounts for initial static deformation. Because the mass in Figure 1, if left unguided, would deviate from ideal rectilinear motion along some unpredictable path, we characterize its average response in terms of an equivalent guided SDOF system having an effective dynamic mass of generalized weight  $P^*$ . The solution for the case when the system properties of  $K$  and  $D$  remain constant can be found in almost any text on vibration theory [3,9].

The steady-state response of the system to a forced periodic base disturbance is characterized by transmissibility as a function of forcing frequency  $f$ . The absolute transmissibility  $Tr_a$  is the ratio between the response amplitude and the disturbance amplitude. Knowing the form of  $Tr_a$  is useful in comparing theory with experimental data obtained by recording system input and output with respect to a stationary global reference. The relative transmissibility  $Tr_r$  is the ratio between the amplitude of the response minus the disturbance, and the disturbance amplitude. Knowing the form of  $Tr_r$  is useful when accounting for changes in material properties associated with the amplitude of cyclic deformation or rate of deformation.

A system with linear restoring forces and linear viscous dissipation forces, subjected to the harmonic disturbance

$$y(t) = Y \sin(2\pi ft); \quad Y = \frac{gG}{(2\pi f)^2} \quad (2)$$

would transmit the disturbance into response according to the expressions

$$Tr_a = \frac{X}{Y} = \frac{\dot{X}}{\dot{Y}} = \frac{\ddot{X}}{\ddot{Y}} = \sqrt{\frac{1 + (2\rho f/f_n)^2}{(1 - [f/f_n]^2)^2 + (2\rho f/f_n)^2}} \quad (3)$$

and

$$Tr_r = \frac{Z}{Y} = \frac{\dot{Z}}{\dot{Y}} = \frac{\ddot{Z}}{\ddot{Y}} = \frac{(f/f_n)^2}{\sqrt{(1 - [f/f_n]^2)^2 + (2\rho f/f_n)^2}} \quad (4)$$

where  $X$ ,  $Y$ , and  $Z$  are amplitudes of  $x(t)$ ,  $y(t)$ , and  $x(t) - y(t)$ , respectively. The “dots” denote differentiation. The equation for  $Y$  is useful when the disturbance is induced by a controlled acceleration of fixed amplitude in terms of a fraction  $G$  of gravity.

The response characteristics are the system's natural frequency  $f_n$  and the fraction  $\rho$  of critical damping. When the properties of  $K$  and  $D$  remain constant,  $f_n$  and  $\rho$  depend only on  $P^*$ . The response characteristics would remain independent of changes in the disturbance amplitude. In the case of nonlinear systems, Equation (I) can at best be solved approximately.

The method we propose is to treat a nonlinear system at each condition of fixed  $G$  and  $f$  as being equivalent to a linear system whose properties depend on the static deformation resulting from  $P$  and on the average dynamic deformation characterized by the undamped free vibration velocity amplitude  $\dot{Z}^*$  predicted by  $G$  and  $f$ . Transmissibilities  $Tr_a$  and  $Tr_r$  are predicted using Equations (3) and (4), respectively, where  $f_n$  and  $\rho$  are first equated to the nonlinear system characteristics  $f_n^*$  and  $\rho^*$ , respectively, given by

$$f_n^* = \frac{1}{2\pi} \sqrt{\frac{K^*(P, \dot{Z}^*)g}{P^*}} \quad (5)$$

and

$$\rho^* = \frac{D^*(P, \dot{Z}^*)}{2} \sqrt{\frac{g}{K^*(P, \dot{Z}^*)P^*}} \quad (6)$$

where  $K^*$  and  $D^*$  are expressions for the average nonlinear stiffness and damping, respectively. Under conditions where  $P^* = P$  and  $\lim_{G \rightarrow 0}$ , Equations (5) and (6) reduce to expressions predicted by linear theory.

### Empirical Stiffness and Damping Formulas

The transmissibility of our nonlinear system approaches that of a linear system as the forcing amplitude decreases; the case  $\lim_{G \rightarrow 0}$  is called the zero amplitude condition. The nonlinear system response would depend on the system stiffness and damping resulting from initial deformation at static equilibrium.

Because corrugated fiberboard is highly sensitive to loading rate, its load–deformation curve from a compressive strength test is a poor predictor of stiffness. In addition, inelastic deformation of material around the horizontal score-line of a container complicates establishing a practical origin of the curve for light loads. An undamped cyclic load–deformation curve can be more accurately predicted from the relationship between  $K$  and  $P$ .

In previous research [8], the top-to-bottom stiffness of a corrugated fiberboard container was found to vary empirically with the compression caused by a static equilibrium load according to the formula

$$K(P) = K_w \left( \frac{P}{W} \right)^r \quad (7)$$

where  $IC_w$  is the stiffness at the unit weight  $W$  per container. In a stack of containers,  $P$  becomes a multiple of  $W$ . Subscript  $w$  is used here to denote parameter values whenever  $P = W$  and therefore indicates the unit weight condition.

Exact damping is difficult to characterize and is often found to be a combination of multiple mechanisms, sometimes interacting with stiffness. General systems with nonlinear damping have been reported to behave like systems with an equivalent linear viscous damping that decreases with an increasing forcing amplitude and also with increasing material stress [3]. Assuming that the same approximation can be applied to corrugated fiberboard, we therefore characterize the damping in a corrugated container at low forcing amplitudes as being a  $P$ -dependent or an equivalent  $IC$ -dependent viscous damping.

$$D(P) = \begin{cases} D_w(P/W)^R & (r = 0) \\ D_w[K(P)/K_w]^{R/r} & (r \neq 0) \end{cases} \quad (8)$$

Given a stack of containers, positive exponents  $r$  and  $R$  would quantify the rates of increase in container stiffness and damping, respectively, when moving from the top to bottom tiers of the stack. The values of  $K(P)$ ,  $K_w$ ,  $D(P)$ , and  $D_w$  so far discussed are considered to be linear properties at the zero amplitude condition.

Applying Equation (5) to the case of linear conditions and incorporating Equation (7) yield the natural frequency as a function of static load

$$f_n(P) = f_w \left( \frac{P}{W} \right)^{(r-1)/2} \quad (9)$$

where

$$f_w = \frac{1}{2\pi} \sqrt{\frac{K_w g}{W^*}} \quad (10)$$

is the natural frequency of the generalized unit weight,  $W^*$ , system at the zero amplitude condition. Applying Equation (6) likewise and incorporating Equation (8) yield

$$\rho(P) = \rho_w \left( \frac{P}{W} \right)^{R-(r+1)/2} \quad (11)$$

where

$$\rho_w = \frac{D_w}{2} \sqrt{\frac{g}{K_w W^*}} \quad (12)$$

is the fraction of critical damping in the generalized unit weight system at the zero amplitude condition.

Increasing the steady state vibration forcing amplitude beneath a corrugated container system has been observed to decrease resonant frequency and sometimes transmissibility [4,7]. To determine how  $K$  and  $D$  might further depend on  $G$ , we first need to examine the force–deformation relationship predicted by Equation (7).

### Force–Deformation Relationship

At an arbitrary state of container deformation  $z$  and corresponding restoring force  $P_s$ , Equation (7) predicts the container stiffness

$$K(P_s) = \frac{dP_s}{dz} = K_w \left( \frac{P_s}{W} \right)^r \quad (13)$$

Rearranging terms and integrating the result yield an equation that can be evaluated to determine the form of the function  $P_s(z)$ .

$$\int \frac{dP_s}{P_s^r} = \frac{K_w}{W^r} \int dz \quad (14)$$

The relationship between  $P_s$  and  $z$ , shown in Figure 2 and given in Table 1, incorporates a reference state of zero deformation at  $P_s = W$ .

When  $r > 0$ , the  $P_s(z)$  relationship exhibits a forever increasing slope. For comparison, Figure 2 also shows the form of a stiffening force–deformation curve. Stiffening and softening systems have been examined with respect to odd function curves symmetric about the origin [3]. If the origin is repositioned at the point corresponding to equilibrium deformation  $z_e$ , the  $P_s(z)$  curve behaves like a stiffening system when  $z > z_e$  and like a softening system when  $z < z_e$ .

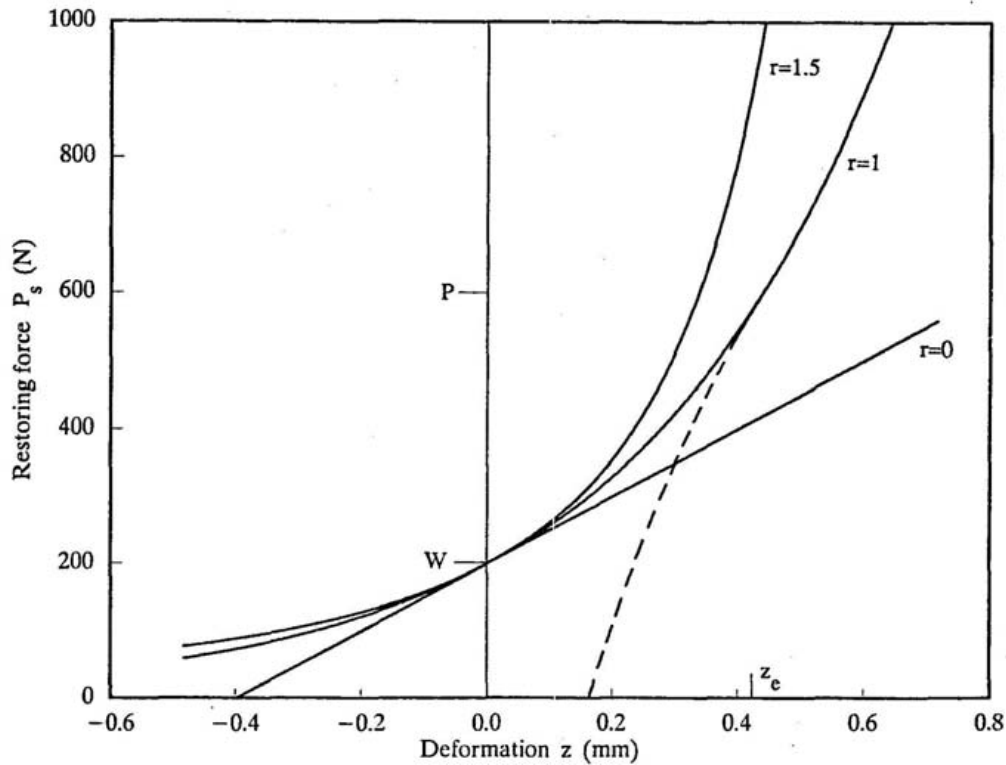


Fig. 2 —Force–deformation curves (solid lines) predicted by Equation (7) for three levels of  $r$  with  $W = 200 \text{ N}$ ,  $K_w = 500 \text{ kN/m}$ , and  $P/W = 3$ . A stiffening system (dashed line) is shown as an extension of the  $P_s(z)$  curve with  $r = 1$ .

Table 1 —Determination of  $P_s(z)$  From Integral Expression

$$\int dP_s/P_s^r = (K_w/W^r) \int dz$$

Exponent	Constraint	$P_s(z)$	$z(P_s)$
$0 \neq r < 1$	$z > \frac{W}{(r-1)K_w}$	$W \left[ (1-r) \frac{K_w}{W} z + 1 \right]^{1/(1-r)}$	$\frac{W}{(1-r)K_w} \left[ \left( \frac{P_s}{W} \right)^{1-r} - 1 \right]$
$r = 0$	$z > -\frac{W}{K_w}$	$W \left[ \frac{K_w}{W} z + 1 \right]$	$\frac{W}{K_w} \left[ \frac{P_s}{W} - 1 \right]$
$r = 1$	—	$W e^{K_w z/W}$	$\frac{W}{K_w} \ln \left( \frac{P_s}{W} \right)$
$r > 1$	$z < \frac{W}{(r-1)K_w}$	$W \left[ (1-r) \frac{K_w}{W} z + 1 \right]^{1/(1-r)}$	$\frac{W}{(1-r)K_w} \left[ \left( \frac{P_s}{W} \right)^{1-r} - 1 \right]$

Integration constant is determined from  $P_s = W$  at  $z = 0$ .

Table 2 –Determination of  $E_s(z)$  From Integral Expression

$$E_s(z) = \int_0^z P_s(z) dz$$

Exponent	Constraint	$E_s(z)$	$E_s(z_e)$
$0 \neq r < 1$	$z > \frac{W}{(r-1)K_w}$	$\frac{W^2}{(2-r)K_w} \left\{ \left[ (1-r) \frac{K_w}{W} z + 1 \right]^{(2-r)/(1-r)} - 1 \right\}$	$\frac{W^2}{(2-r)K_w} \left[ \left( \frac{P}{W} \right)^{2-r} - 1 \right]$
$r = 0$	$z > -\frac{W}{K_w}$	$\frac{W^2}{K_w} \left[ \frac{1}{2} \left( \frac{K_w}{W} z \right)^2 + \frac{K_w}{W} z \right]$	$\frac{W^2}{2K_w} \left[ \left( \frac{P}{W} \right)^2 - 1 \right]$
$r = 1$	—	$\frac{W^2}{K_w} \left( e^{zK_w/W} - 1 \right)$	$\frac{W^2}{K_w} \left[ \frac{P}{W} - 1 \right]$
$1 < r \neq 2$	$z < \frac{W}{(r-1)K_w}$	$\frac{W^2}{(2-r)K_w} \left\{ \left[ (1-r) \frac{K_w}{W} z + 1 \right]^{(2-r)/(1-r)} - 1 \right\}$	$\frac{W^2}{(2-r)K_w} \left[ \left( \frac{P}{W} \right)^{2-r} - 1 \right]$
$r = 2$	$z < \frac{W}{K_w}$	$-\frac{W^2}{K_w} \ln \left( 1 - \frac{K_w z}{W} \right)$	$\frac{W^2}{K_w} \ln \left( \frac{P}{W} \right)$

Integration constant is determined from  $E_s = 0$  at  $z = 0$ .

The elastic energy  $E_s$  caused by deformation is determined with respect to a state of zero elastic energy at  $P_s = W$  from the expression

$$E_s(z) = \int_0^z P_s(z) dz \quad (15)$$

Equation (15) is evaluated in Table 2.

### Free Vibration Response

Consider the motion of the mass between the positions of minimum deformation  $z_i$  and maximum deformation  $z_j$  about the static equilibrium deformation  $z_e$ . The total potential energy  $U_p$  in the system caused by elastic deformation plus work against gravity depends on  $z$  according to

$$U_p(z) = E_s(z) - E_s(z_e) + Pz_e - Pz \quad (16)$$

At the top of its relatively upward stroke from static equilibrium to deformation  $z_i$ , the system attains a state of energy equivalent to the size of the area  $U_i$  shown in Figure 3. A second state of energy, equivalent to the size of area  $U_j$ , accumulates at the bottom of the relatively downward stroke at deformation  $z_j$ . The kinetic energy  $U_k$  in the system is given by

$$U_k(z) = \frac{P^*}{2g} \left( \frac{dz}{dt} \right)^2 \quad (17)$$

Consider next the motion of the mass during undamped free vibrations. The sum of system potential energy and kinetic energy remains constant such that

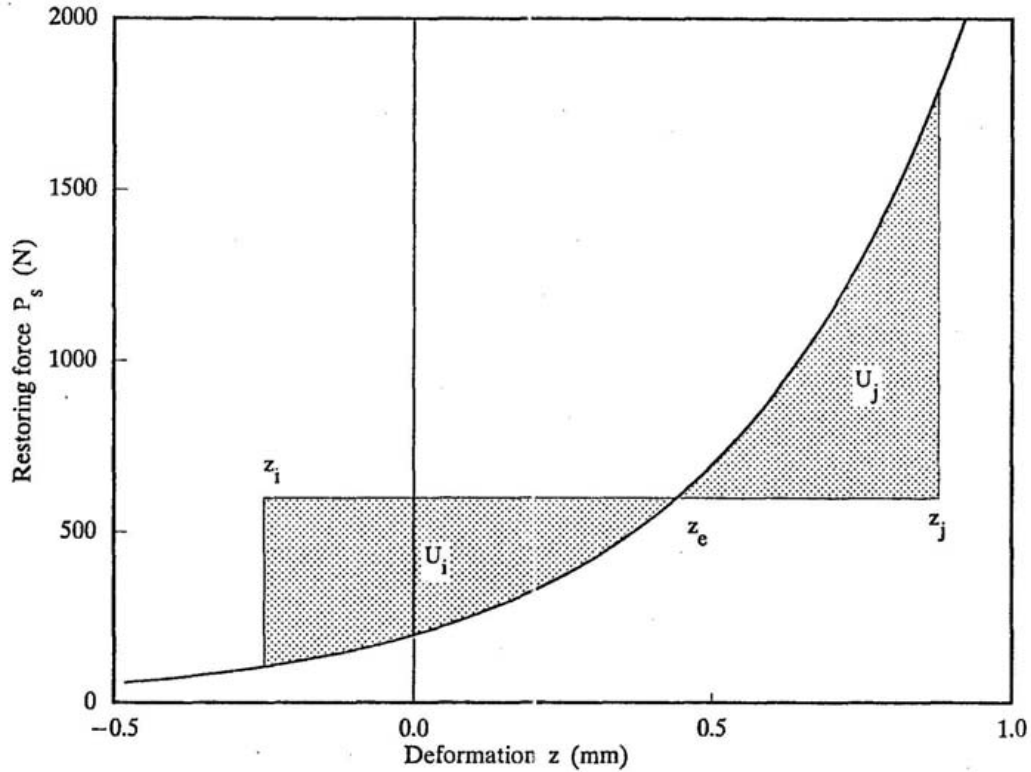


Fig. 3—Comparison between areas  $U_i$  and  $U_j$  corresponding to potential energy in system at deformations  $z_i$  and  $z_j$ , respectively, when  $W = 200 \text{ N}$ ,  $K_w = 500 \text{ kN/m}$ ,  $P/W = 3$ , and  $r = 1$ .

$$U_k(z) = U_p(z_i) - U_p(z) \quad (18)$$

and

$$U_k(z_e) = U_i = U_j = \frac{P^*}{2g} \dot{Z}^{*2} \quad (19)$$

where  $\dot{Z}^*$  becomes the maximum undamped free vibration velocity of the nonlinear system. The motion of a nonlinear system will obviously be highly nonharmonic, yielding  $z_e - z_i \neq z_j - z_e$ . However, the maximum velocity during the upward stroke and the maximum velocity during the downward stroke will remain equal.

If the amplitude of the system is thus characterized in terms of  $\dot{Z}^*$ , then corresponding deformations  $z_i$  and  $z_j$  need to be determined. To do this, we first equate the combined sides of Equation (16) to zero to define

$$Q_0(z) = E_s(z) - E_s(z_e) - U_p + Pz_e - Pz = 0 \quad (20)$$

We then incorporate Equation (20) and its partial derivative  $\partial Q_0/\partial z$  within Newton's algorithm for determining a root  $z$ , given  $U_p$ . The result is

$$z_{n+1} = z_n - \frac{E_s(z_n) - E_s(z_e) - U_p - Pz_n + Pz_e}{P_s(z_n) - P} \quad (21)$$

Equation (21) is solved by updating  $z_n$  until convergence. Given  $\dot{Z}^*$  and determining  $U_p = U_i = U_j$  from Equation (19), an initial estimate of  $z_n < z_e$  will converge to  $z_i$ . An initial estimate of  $z_n > z_e$  will converge to  $z_j$ .

The free vibration natural period  $p$  can be determined from the elapsed time between minimum and maximum deformations. Combining Equation (17) with Equation (18) and rearranging terms yield

$$\frac{dz}{dt} = \sqrt{\frac{2g}{P^*}} \sqrt{U_p(z_i) - U_p(z)} \quad (22)$$

Substituting Equation (16) into the result and again rearranging terms lead to an expression for the differential elapsed time  $dt$  during the undamped free vibration.

$$dt = \frac{1}{\sqrt{2}} \frac{1}{2\pi f_w} \sqrt{\frac{P}{W}} Q_1(z) dz \quad (23)$$

Here  $f_w$  is given by Equation (10) and

$$Q_1(z) = \frac{1}{\sqrt{E_s(z_i)/K_w - E_s(z)/K_w + W/K_w(P/W)(z - z_i)}} \quad (24)$$

Integrating both sides of Equation (23) between the limits corresponding to the initial and final conditions of time and deformation over a half-cycle of free vibration yields the system natural half-period. The system natural period is thus expressed as a function of  $\dot{Z}^*$  by writing

$$p(\dot{Z}^*) = 2 \int_0^{p/2} dt = \frac{1}{\sqrt{2}} \frac{1}{\pi f_w} \sqrt{\frac{P}{W}} \int_{z_i}^{z_j} Q_1(z) dz \quad (25)$$

where the integration limits  $z_i$  and  $z_j$  are determined using Equation (21).

The function  $Q_1(z)$  needs to be integrated numerically after substituting the terms from Table 2 into Equation (24). Function  $Q_1(z)$  becomes singular at the integration limits. However, the function can still be integrated by applying an adaptive quadrature algorithm and weighting function [10]. The result is

$$\bar{Q}_1(\dot{Z}^*) = \int_{z_i}^{z_j} Q_1(z) dz \approx \frac{z_j - z_i}{2} \frac{\pi}{m+1} \sum_{n=0}^m \xi'_n Q_1\left(\frac{(z_i + z_j) + (z_j - z_i)\xi_n}{2}\right) \quad (26)$$

where

$$\xi_n = \cos\left(\frac{2n+1}{m+1} \frac{\pi}{2}\right); \quad \xi'_n = \sin\left(\frac{2n+1}{m+1} \frac{\pi}{2}\right) \quad (n = 0, \dots, m) \quad (27)$$

The nonlinear system natural frequency  $f_n^*$  is thus calculated from

$$f_n^*(\dot{Z}^*) = \frac{1}{p(\dot{Z}^*)} = \frac{\sqrt{2}\pi f_w}{\sqrt{(P/W)\bar{Q}_1(\dot{Z}^*)}} \quad (28)$$

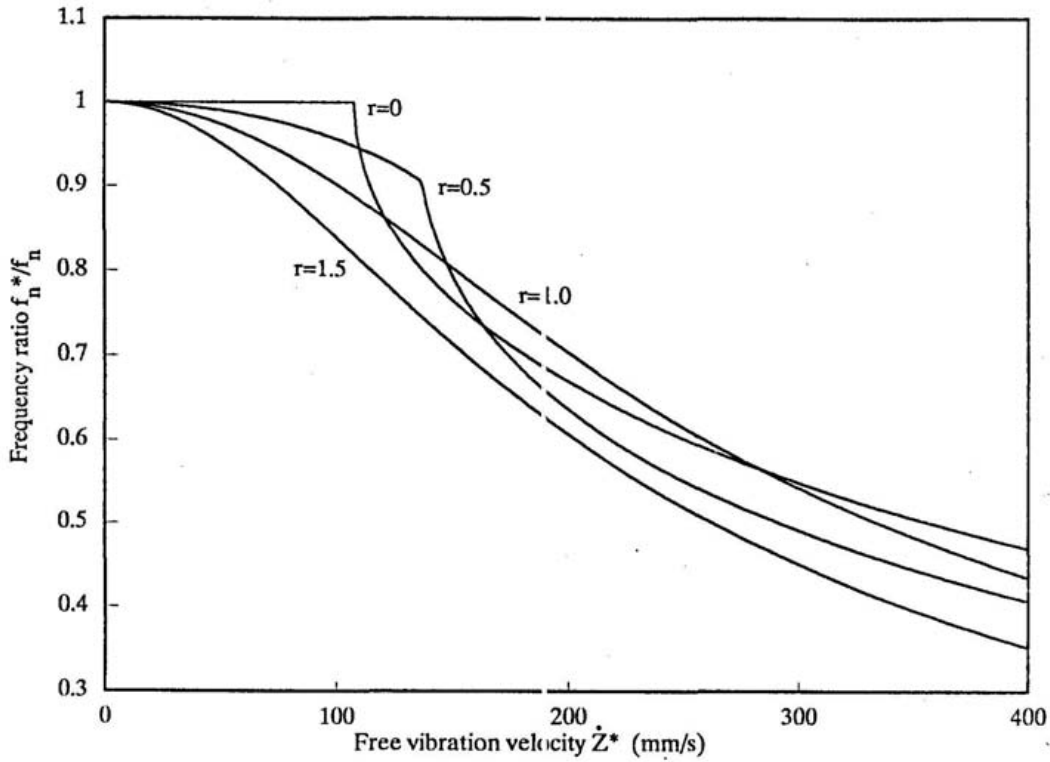


Fig. 4 —Plots of frequency ratio  $f_n^*/f_n$  as a function of  $\dot{Z}^*$  for four levels of  $r$  with  $W = 200\text{ N}$ ,  $K_w = 500\text{ kN/m}$ , and  $P/W = 3$ .

Figure 4 illustrates how the frequency ratio  $f_n^*/f_n$  depends on  $\dot{Z}^*$  for various levels of  $r$ . The knees in the curves with  $r < 1$  occur at the  $z$  constraints of the  $P_s(z)$  curves (Table 1), below which  $P_s = 0$ . As  $\dot{Z}^*$  approaches zero, the value of  $f_n^*$  predicted by Equation (28) converges to the prediction by Equation (9). From Equation (24), it is seen that the nonlinear system value of  $\bar{Q}_1$  cannot be determined when  $\dot{Z}^* = 0$  and  $z = z_i$  using Equation (26). However, equating Equations (9) and (28) yields

$$\bar{Q}_1(0) = \frac{\sqrt{2}\pi}{(P/W)^{r/2}} \quad (29)$$

### Forced Vibration Response

Stiffness continuously changes with deformation. An average value of  $K^*(P, \dot{Z}^*)$  can be determined from the stiffness of an equivalent linear system subjected to a precompression  $P$  and having an equal natural frequency  $f_n^*$ .

$$K^*(P, \dot{Z}^*) = \frac{P^s}{g} \left[ 2\pi f_n^*(\dot{Z}^*) \right]^2 \quad (30)$$

We next incorporate the damping relationship at the zero amplitude condition proposed in Equation (8) to examine its application to higher velocity amplitude levels. We therefore estimate an average value of  $D^*(P, \dot{Z}^*)$  in terms of the corresponding stiffness  $K^*$ .

$$D^*(P, \dot{Z}^*) = \begin{cases} D_w(P/W)^R & (r = 0) \\ D_w[K^*(P, \dot{Z}^*)/K_w]^{R/r} & (r \neq 0) \end{cases} \quad (31)$$

An average  $\rho^*$  is thus given by Equation (6).

Consider now the damped system subjected to a forced periodic base disturbance characterized by Equation (2). Differentiating Equation (2) with respect to time yields the velocity amplitude  $\dot{Y}$  of the forcing disturbance in terms of a fixed  $G$  and  $f$ .

$$\dot{Y} =: \frac{gG}{2\pi f} \quad (32)$$

Substituting Equation (32) into Equation (4) gives an expression for predicting the forced relative velocity response of a linear system in terms of constant system characteristics.

$$\dot{Z} = \frac{gG}{2\pi f} \frac{(f/f_n)^2}{\sqrt{[1 - (f/f_n)^2]^2 + (2\rho f/f_n)^2}} \quad (33)$$

To predict the response of a nonlinear system whose forced response characteristics depend on system input at  $G$  and  $f$ , we treat the system as being equivalent to a linear system having equal free vibration response characteristics, such that

$$\begin{aligned} \dot{Z} &= \dot{Z}^* \\ f_n &= f_n^* \\ \rho &= \rho^* \end{aligned} \quad (34)$$

Combining Equations (33) and (34) produces an equation whose roots correspond to an approximate velocity amplitude of the nonlinear system.

$$Q_2(\dot{Z}^*) = \frac{(f/f_n^*)^2}{\sqrt{[1 - (f/f_n^*)^2]^2 + (2\rho^* f/f_n^*)^2}} - \dot{Z}^* \frac{2\pi f}{gG} = 0 \quad (35)$$

The roots must also satisfy Equations (5) and (6), using Equations (28), (30), and (31), and thus yield unique system response characteristics for each fixed  $G$  and  $f$ . The form of Equation (35) and the multiple roots that might occur are shown in Figure 5. Given  $f_n^*$  and  $\rho^*$  as functions of  $G$  and  $f$ , the nonlinear transmissibilities  $\text{Tr}_a^*$  and  $\text{Tr}_r^*$  are thus defined in terms of equivalent expressions for a linear system from

$$\text{Tr}_a^*(G, f) = \sqrt{\frac{1 + (2\rho^* f/f_n^*)^2}{[1 - (f/f_n^*)^2]^2 + (2\rho^* f/f_n^*)^2}} \quad (36)$$

and

$$\text{Tr}_r^*(G, f) = \frac{(f/f_n^*)^2}{\sqrt{[1 - (f/f_n^*)^2]^2 + (2\rho^* f/f_n^*)^2}} \quad (37)$$

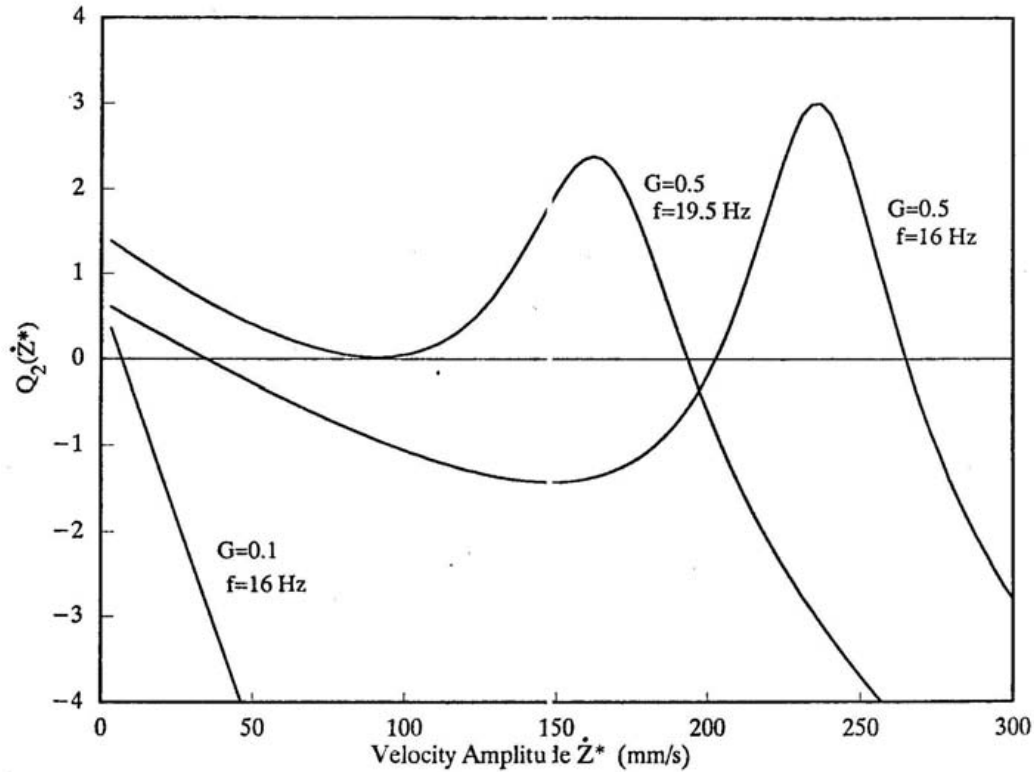


Fig. 5 —Plots of  $Q_2$  versus  $\dot{Z}^*$  for two levels of  $G$  and  $f$  with  $W = 200\text{ N}$ ,  $K_w = 500\text{ kN/m}$ ,  $P/W = 3$ ,  $r = 1$ ,  $R = 1$ , and  $\rho_w = 0.1$ .

Examples of Equation (36) are plotted in Figure 6. The higher roots of Equation (35) that correspond to physically unattainable conditions are rejected. The case shown for  $G = 0.5$  behaves like a softening system and exhibits the classical unstable frequency region and jump phenomenon.

## TEST PROCEDURE

### Material

Seven replicated sets of regular slotted-style boxes having scored and folded interior end-pads and fabricated according to the  $2^3$  full-factorial combinations of two flute constructions, two box sizes, and two end-pad clearances were evaluated. Boxes were fabricated from material of either nominal 1.4-GPa (200-lb/in<sup>2</sup>) bursting strength B-flute single-wall or 2.4-GPa (350-lb/in<sup>2</sup>) bursting strength BC-flute double-wall corrugated fiberboard construction. The exterior box dimensions were fixed at either nominally 305 mm long by 215 mm wide by 215 mm high or 430 by 305 by 215 mm. The purpose was to provide boxes that could be internested and stacked for an anticipated future study.

End pads of 1.4-GPa C-flute material were fabricated to a height, with respect to the interior depth dimension of each box grade, to produce two levels of load sharing with the box (Fig. 7). A pair of zero-clearance end-pads contributed to a state of continuous load sharing with the box. An alternate pair of end-pads, cut 4.7 mm shorter, contributed an intermittent load sharing, depending on the box load.

All materials were preconditioned in a dry environment below 30 percent relative humidity (RH), then conditioned and tested under standard conditions of 23°C (73°F) and 50 percent RH. The top-to-bottom

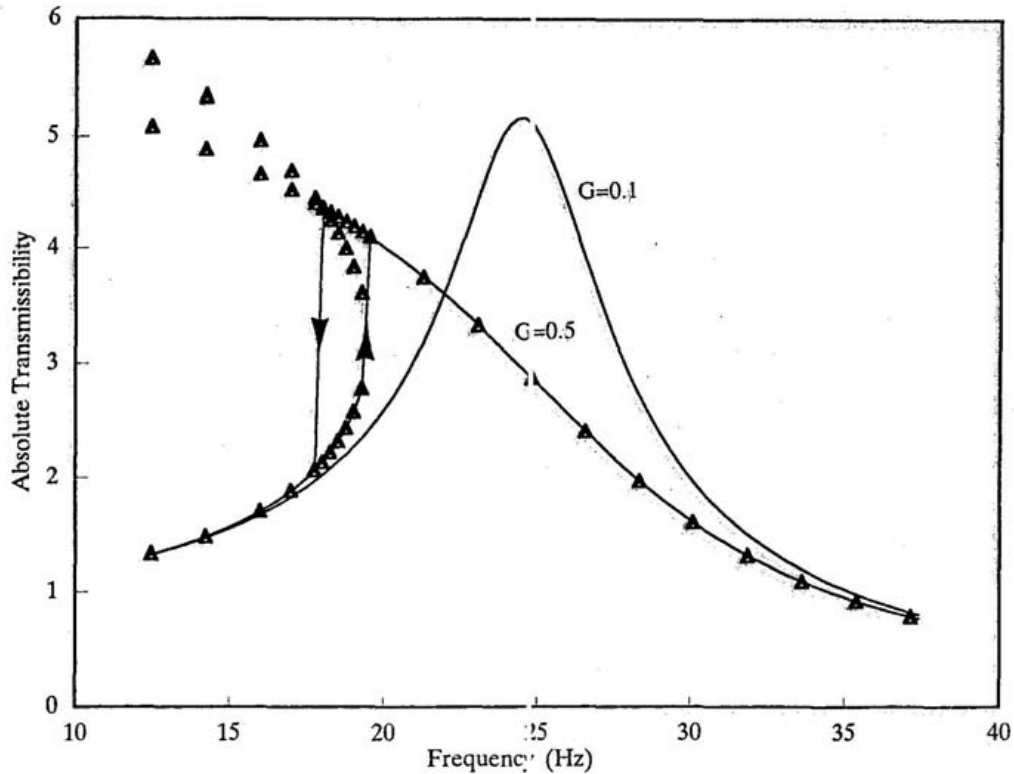


Fig. 6—Plot of absolute transmissibility as a function of forcing frequency predicted by Equation (36) for two levels of  $G$ . The points correspond to roots of the  $Q_2$  function (Equation (35)). The lines are physically attainable transmissibility curves occurring during increasing frequencies (up arrow) or decreasing frequencies (down arrow).  $W = 200 \text{ N}$ ,  $K_w = 500 \text{ kN/m}$ ,  $P/W = 3$ ,  $r = 1$ ,  $R = 1$ , and  $\rho_w = 0.1$ .

compression strengths of the empty boxes without end pads, based on an average of five samples, were nominal 305-mm B-flute, 3.35 kN; nominal 430-mm B-flute, 3.91 kN; nominal 305-mm BC-flute, 6.36 kN; and nominal 430-mm BC-flute, 8.38 kN.

### Test Conditions

Each box with end pads of the factorial combinations comprised the spring element of a spring-mass system subjected to a sinusoidal, swept frequency, forced vibration (Fig. 8). Each spring element specimen was subjected to nine test conditions: top loading at three levels of an imposed mass combined with three levels of a constant forcing acceleration amplitude.

Top loads of 294, 516, and 739 N were used with the nominal 305-mm-long boxes, and top loads of 418, 743, and 1,070 N with the nominal 430-mm-long boxes. These load levels were selected to achieve an overall compromise involving box strength, induced stiffness nonlinearity, and end pad load sharing considerations and to approximate the same relative load per perimeter between the two box sizes.

The forcing vibration was a controlled acceleration wave having a constant zero-to-peak amplitude of either 1/16, 1/8, or 1/4  $g$ . The upper  $G$ -level was chosen so as not to induce a repetitive bouncing action. Seven replicates of the  $2^3$  experimental design, with each element subjected to nine test conditions, yielded 504 experimental transmissibility curves for comparison with our theory.

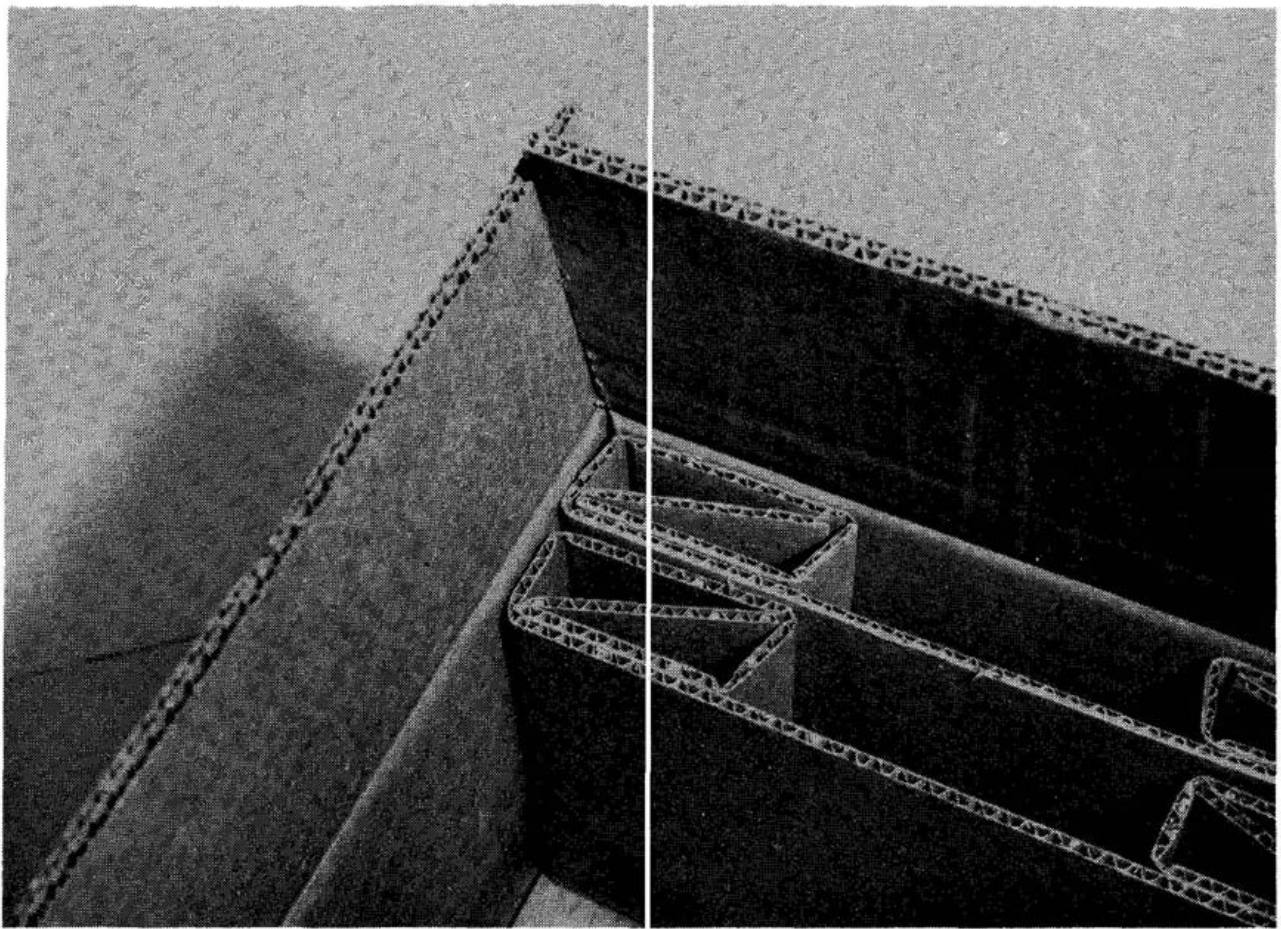


Fig. 7 —View of box specimen interior showing relative height difference between two end-pads. (M88 0262-15)

### **Vibration Wave**

Each spring-mass system was positioned unrestrained upon the previously described force plate system [11], which was vibrated by an electrohydraulic vibration table. In this forced disturbance system, the controlled acceleration of the force plate becomes the input and the specimen reaction force sensed by the force plate becomes the output. The force plate system design is such that the forces resulting from plate static weight and plate inertial acceleration are subtracted out.

The input vibration was a constant amplitude acceleration with the frequency sweeping between 10 and 30 Hz at the logarithmic rate of 0.1 decade per second (4.7 s per sweep half-period). To streamline the analysis and to work with only the lowest root of  $Q_2$  in matching predicted transmissibility curves with data, we used data from only the increasing sweep.

### **Data Acquisition and Vibration Control**

Data were acquired using a unique software system to simultaneously control the force plate vibration and record its induced acceleration and responding reaction force. A calibrated open loop control system was achieved by exporting a mathematically generated time sequence of digitized voltage values; i.e., a control signal, through a microcomputer digital to analogue conversion hardware, which made the microcomputer perform like a function generator. At the same time, the force plate acceleration and reaction force signals were imported through the microcomputer analogue to digital hardware and recorded in digital format.

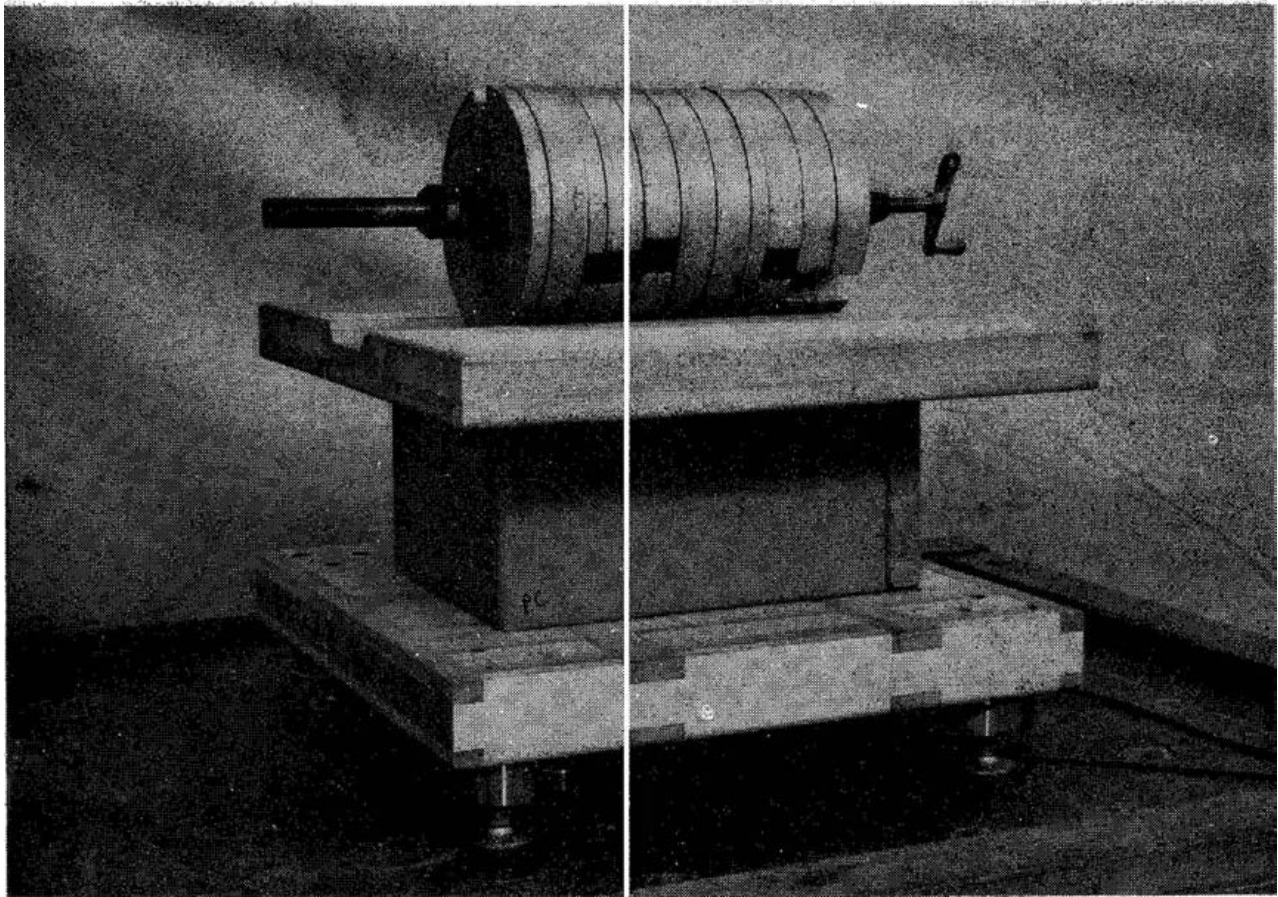


Fig. 8 —Test specimen loaded on force plate and functioning as spring component in SDOF system. (M90 0008-4)

The control signal was compared with the force plate acceleration and then amplified or attenuated as needed until a swept frequency signal of finite duration could be exported, with the result being a swept frequency force plate acceleration having a constant amplitude. The acceleration and force signals were left unfiltered. To overcome the interference caused by noisy signals and to characterize a nonharmonic signal amplitude, the root mean square (RMS) amplitude of each sweeping sinusoid of the swept sine signals were first calculated, then multiplied by  $\sqrt{2}$ , to determine the equivalent noise-free sinusoidal amplitude at each frequency. Data at each load level  $P$  in the form of force plate acceleration amplitude  $G$  and specimen reaction force amplitude  $F$ , at each instantaneous forcing frequency  $f$ , were retained for generation and analysis of the transmissibility curves.

The advantage of using a single software system for simultaneous electrohydraulic system control and data acquisition is that the exact time and frequency characteristics of the control signal are known as a reference for making calculations with the acceleration and force data,

## RESULTS

### Fit of Theoretical Transmissibility Curves to Experimental Data

Zero amplitude, unit weight system characteristics  $f_w$  and  $\rho_w$ , unit dynamic weight  $W^*$ , and material properties  $r$  and  $R$  of each flute construction, box size, and end-pad clearance combination were determined by fitting theoretical transmissibility curves to data. Data comprising the three  $P$ -levels and three  $G$ -levels were pooled to characterize each replicated specimen. Experimental observations  $P$ ,  $G$ ,  $F$ , and  $f$  provided input to the regression formula

$$\frac{\ddot{X}}{\ddot{Y}}P^* = \frac{F}{G} = W^* \left( \frac{P}{V\tau} \right) \text{Tr}_a^*(f_w, \rho_w, r, R) \quad (38)$$

derived by equating Equation (3) to (36) and multiplying through by  $P^*$ . With the given  $f_w$ ,  $\rho_w$ , and  $W^*$ , the zero-amplitude, unit weight material properties  $K_w$  and  $D_w$  are calculated from the expressions

$$K_w = 4 \frac{W^*}{g} - (\pi f_w)^2 \quad (39)$$

and

$$D_w = 2\rho_w \sqrt{\frac{K_w W^*}{g}} \quad (40)$$

The five-parameter Equation (38) was found to work well in a nonlinear regression program provided that good initial estimates of its parameters are supplied. This required the division of each data set into subsets, broken down by  $P$ , for each of which  $K(P)$ ,  $D(P)$ , and  $P^*$  could be determined, assuming linear behavior at  $r = 0$  and  $R = 0$ . Fitting Equations (7) and (8) to the results of the subset analysis yielded initial estimates of nonlinear stiffness properties  $K_w$  and  $r$ , and nonlinear damping properties  $D_w$  and  $R$ , respectively. Finally, initial estimates of  $f_w$  and  $\rho_w$  were determined using Equations (10) and (11), respectively.

### Corrugated Container Properties

The results of the replicate regression analyses are given in Table 3. To compare all materials at an equal load level, zero amplitude values of  $f_w$ ,  $\rho_w$ ,  $K_w$ , and  $D_w$  are given at  $P = 194$  N, a load found to maximize the observed score-line phenomenon with respect to box size. The system characteristics and material property data were averaged and subjected to the usual methods of factorial analysis to identify significant effects and interactions among the experimental variables. Figure 9 shows variation in stiffness. Based on main effects, the weaker B-flute construction yielded significantly stiffer boxes, implying that material deformation around the horizontal score-line has a greater effect on box compression stiffness than does panel flexural stiffness. However, a general statement about the effect of flute construction on stiffness needs to address the interaction with box size.

Single-wall [12] and double-wall [13] box compression theories predict that the perimeter ratio between the 430-mm boxes and the 305-mm boxes of approximately  $\sqrt{2}$  should yield a strength ratio of approximately 1.18, compared to our experimentally determined strength ratios of 1.17 for the B-flute construction and 1.32 for the BC-flute construction. At the 194-N load level, the ratio of average 430-mm box stiffness to average 305-mm box stiffness (Fig. 9) becomes  $\sqrt{2}$ , thereby predicting the load at which score-line behavior becomes most pronounced.

Table 3 –Response Characteristics and System Properties at 194-N Load Level

Flute type	Nominal size (mm)	End-pad clearance (mm)	$W^*/W$	$f_n(P)$		$r$	$R$	$K(P)$ (kN/m)	$D(P)$ (kN s/m)
				(Hz)	$\rho(P)$				
B	305	4.7	0.906	24.7	0.253	1.28	0.58	433	1.41
			0.894	20.5	0.134	1.16	1.13	490	0.79
			0.837	25.6	0.183	1.06	0.99	430	0.97
			0.818	27.8	0.164	1.35	1.27	495	0.93
			0.843	26.7	0.124	1.28	1.51	472	0.69
			0.819	23.2	0.164	1.36	1.18	344	0.77
			0.865	24.2	0.168	1.31	1.23	397	0.87
			(Average)	0.855	25.2	0.170	1.26	1.13	437
BC	305	4.7	0.766	20.8	0.130	1.10	0.97	260	0.51
			0.947	15.8	0.151	1.40	1.21	184	0.56
			0.817	17.4	0.135	1.32	1.32	194	0.48
			0.834	17.8	0.114	1.29	1.50	208	0.42
			0.814	17.6	0.155	1.34	1.20	198	0.55
			0.877	14.2	0.156	1.52	1.33	139	0.48
			0.861	18.3	0.178	1.21	1.07	226	0.70
			(Average)	0.845	17.4	0.146	1.31	1.23	201
B	430	4.7	0.907	27.4	0.145	0.93	1.04	533	0.90
			0.891	23.5	0.185	0.94	0.88	566	1.16
			0.919	23.1	0.212	0.93	0.78	568	1.36
			0.849	30.1	0.176	0.89	0.86	603	1.12
			0.842	26.8	0.157	0.96	0.97	472	0.88
			0.872	33.6	0.143	0.62	0.91	772	1.05
			0.874	22.6	0.155	1.17	1.12	349	0.76
			(Average)	0.879	23.2	0.168	0.92	0.94	552
BC	430	4.7	0.850	21.1	0.189	0.90	0.84	296	0.84
			0.809	20.0	0.174	1.07	0.94	252	0.70
			0.807	19.6	0.270	1.00	0.61	243	1.06
			0.846	17.3	0.126	1.15	1.14	199	0.46
			0.894	17.1	0.154	1.21	1.08	204	0.58
			0.860	13.2	0.128	1.26	1.21	177	0.44
			0.794	20.4	0.129	0.94	0.88	258	0.52
			(Average)	0.837	13.8	0.167	1.08	0.96	233
B	305	0	0.933	25.1	0.111	1.27	1.39	461	0.64
			0.804	27.2	0.102	1.22	1.17	465	0.55
			0.839	22.7	0.123	1.40	1.26	338	0.58
			0.855	23.6	0.165	1.10	1.08	474	0.93
			0.865	24.8	0.141	1.23	1.20	417	0.75
			0.939	20.9	0.155	1.44	1.40	320	0.75
			0.914	23.8	0.135	1.32	1.33	405	0.73
			(Average)	0.878	24.4	0.133	1.28	1.26	411

Table 3—Response Characteristics and System Properties at 194-N Load Level—con.

Flute type	Nominal size (mm)	End-pad clearance (mm)	$W^*/W$	$f_n(P)$ (Hz)	$\rho(P)$	$r$	$R$	$K(P)$ (kN/m)	$D(P)$ (kN s/m)
BC	305	0	0.801	19.3	0.116	1.27	1.17	234	0.45
			0.912	19.2	0.136	1.16	1.16	263	0.59
			0.802	21.3	0.118	1.03	1.21	284	0.50
			0.794	21.7	0.165	1.06	0.94	293	0.71
			0.824	20.4	0.152	1.07	0.98	268	0.63
			0.843	19.9	0.133	1.08	1.2	261	0.55
			0.738	22.9	0.153	0.94	0.84	302	0.64
(Average)			0.816	20.7	0.139	1.09	1.07	272	0.58
B	430	0	0.883	37.5	0.154	0.68	0.89	972	1.26
			0.855	37.9	0.122	0.68	1.07	960	0.98
			0.872	31.1	0.150	0.88	1.07	661	1.01
			0.853	33.1	0.106	0.79	1.19	731	0.74
			0.908	30.5	0.127	0.86	1.19	663	0.87
			0.905	30.6	0.225	0.86	0.78	665	1.55
			0.794	28.2	0.114	1.01	1.18	496	0.63
(Average)			0.867	32.7	0.142	0.82	1.05	735	1.01
BC	430	0	0.814	23.8	0.192	0.79	0.71	361	0.92
			0.719	21.2	0.129	1.03	0.98	253	0.49
			0.792	23.5	0.147	0.82	0.81	342	0.68
			0.873	21.9	0.124	0.91	1.09	328	0.59
			0.834	27.9	0.196	0.65	0.56	506	1.13
			0.831	21.4	0.158	0.96	0.87	297	0.70
			0.762	24.6	0.182	0.82	0.68	360	0.84
(Average)			0.804	23.5	0.161	0.85	0.82	350	0.76

The flute-size subset averages show that as opposed to the trend observed for strength, the B-flute boxes became stiffer with increasing size to a greater extent than did the BC-flute boxes. General strength observations cannot be relied upon to predict the effect of design characteristics on stiffness.

As expected, the zero clearance end-pads yielded stiffer boxes than did the 4.7-mm shorter pads as a result of initial load sharing (Fig. 9). However, as shown by the size-clearance subset averages, end-pad clearance was found to increase the zero amplitude compression stiffness of the 430-mm box significantly more than that of the 305-mm box. Evaluation of the  $r$ -levels provides an explanation for this effect.

Figure 10 shows how the material property  $r$  was found to depend on the experimental design variables. The 4.7-mm clearance end-pads induced a higher  $r$ -level. The shorter end-pads shared the box compressive load at high loads, but not at low loads. The flute-clearance subset averages show that end-pad clearance had a greater effect on  $r$  for the BC-flute construction material than for the B-flute material. This is consistent with the previous observation that box compression stiffness results primarily from a score-line phenomenon. The correlation between  $r$  and  $K(P)$  predicted at the low load level of  $P = 10$  N, where the correlation is more readily apparent, is further shown in Figure 11. As inferred from a higher  $r$ -level in Figure 10, the 305-mm boxes stiffened with loading at a inherently higher rate than did the 430-mm boxes. The data in Figure 11 indicate a general decrease

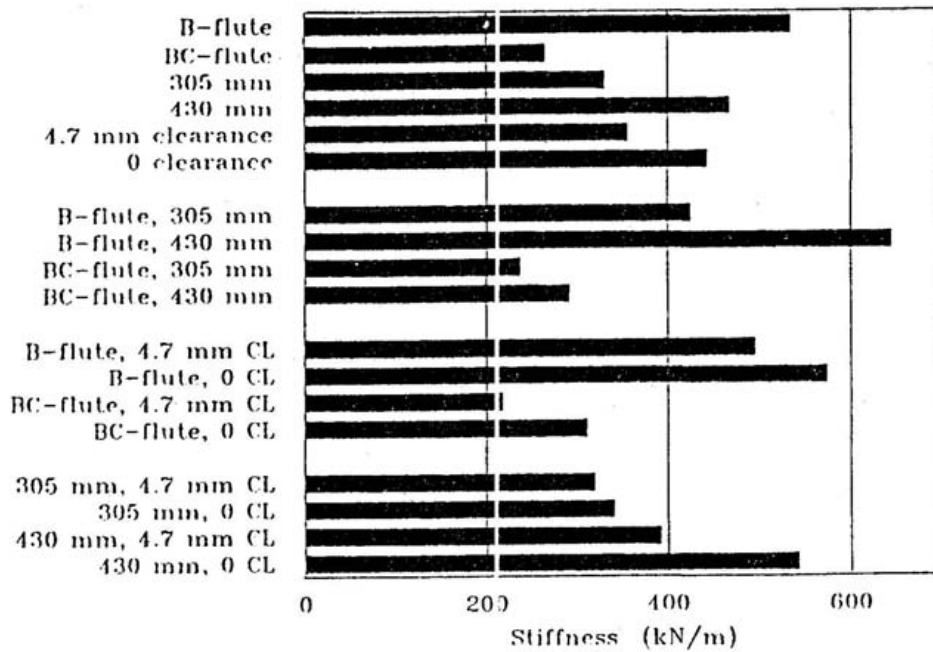


Fig. 9 —Comparison of 194-N load stiffness  $K$  (Table 3) with subset averages resulting from main effects (B- or BC-flute material, 305- or 430-mm box length, and 4.7-mm or 0 end-pad clearance) of experimental design and subset averages resulting from two-way interactions.

in  $r$  with increasing  $K$  and imply that at low loads, a step increase in  $r$  resulting from designing a clearance into the end pads is accompanied by a proportional relative reduction in  $K$ .

Damping properties were found to be more variable than stiffness properties and less sensitive to the effects of the experimental variables. When given an average  $R = 1.061$  and an average  $r = 1.082$ , it is seen from Equation (11) that the damping ratio  $p$  has little dependence on  $P$ . Interestingly, our results yielded an average constant  $p = 0.15$  independent of any effects from the experimental variables and applicable to arbitrary load levels.

The generalized dynamic weight is given in Table 3 as a dimensionless ratio with respect to the  $W$ -level of each test. The effective dynamic weight of each mass following our experimental procedure was found to equal an average of 84 percent, of its static weight. The data indicate a dependence on specimen flute construction and consequently the system resonant frequency. This could have resulted from a data analysis bias resulting from BC-flute specimen resonant frequencies occurring near the upper 30-Hz end of our frequency sweep.

## CONCLUSIONS

A nonlinear theory of forced vibration response has been developed and applied to corrugated fiberboard containers loaded in top-to-bottom cyclic compression. The container response at arbitrary precompression load levels and harmonic forcing accelerations was shown to depend on material stiffness, damping, and the respective rates of load-dependent change. Physical constant: characterizing various container designs were determined by matching theoretical softening system transmissibility curves to data acquired using a force plate excitation-response system. Favorable or detrimental response characteristics of container stacks can be inferred from the nonlinear material properties of individual containers and the property interactions.

The results of previous linear MDOF theory applied to corrugated container stacks predicted the physical properties of individual containers to which the stack response is most sensitive. Given fixed interior cushioning

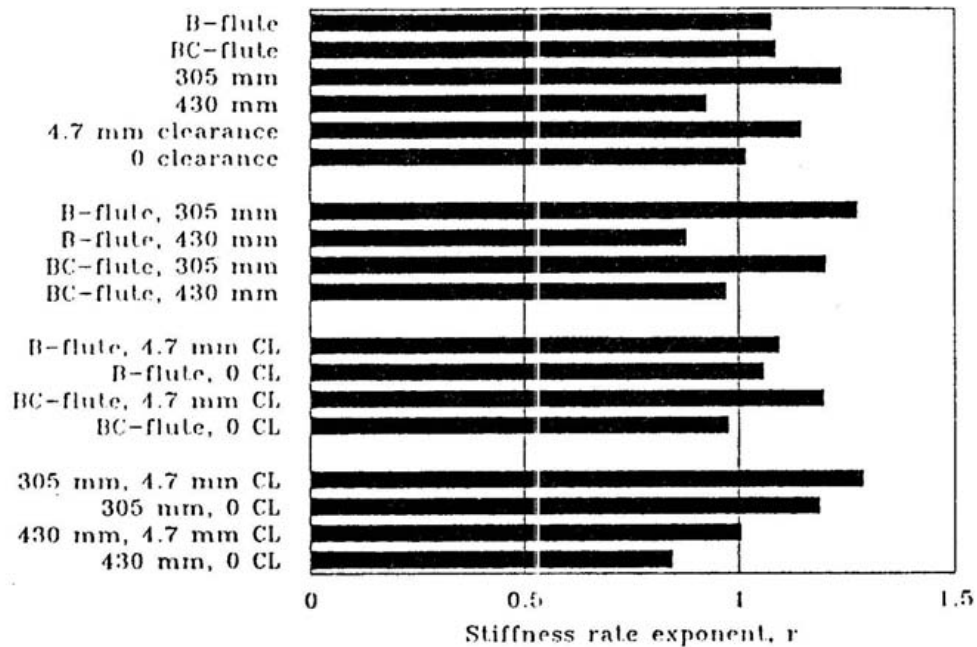


Fig. 10—Comparison of stiffness rate increase exponent  $r$  (Table 3) with subset averages resulting from main effects of experimental design and subset averages resulting from the two-way interactions.

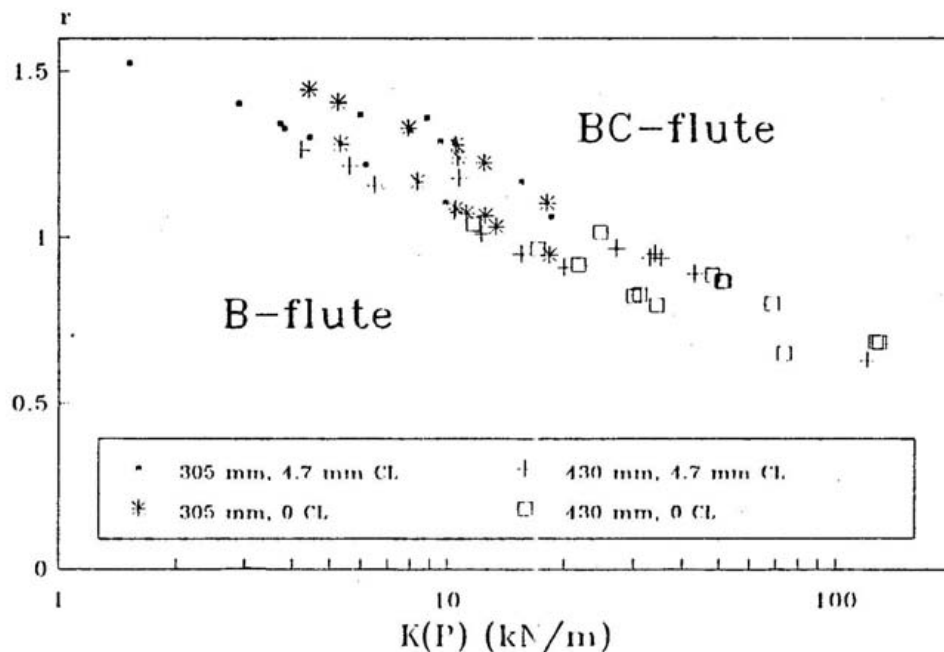


Fig. 11—Comparison between  $r$  and  $K$  predicted at the  $10\text{-}N$  load level from data between  $294\text{-}N$  and  $1070\text{-}N$  load levels.

properties, vibration-sensitive products would favor low stiffness boxes. Vibration resistant products can take advantage of stiff boxes, thereby permitting lower grade containers. The force-deformation response of corrugated containers is highly nonlinear. General products can benefit from container designs that further exaggerate the nonlinear response, reduce product acceleration levels, and reduce stack compressive loads.

The experimental method presented here shows how to characterize individual containers. The results imply how to favorably alter the container design. Single wall corrugated fiberboard construction was shown to yield stiffer boxes than did double-wall construction as a result of suspected inelastic material behavior around the horizontal score-line. Load sharing between the outer box and interior packaging can further stiffen the container. Our study shows how providing a clearance between interior end-pads and the container is one way to control the onset of load sharing and increase the force-deformation nonlinearity. However, in our case, the expected benefits from the end-pad clearance need to be evaluated with the corresponding reduction in stiffness and the interaction with box size.

This study is being extended to characterize the response of container stacks. Our objectives are to improve testing methods and to gain a better understanding of vibration protection.

## REFERENCES

1. ASTM, "Standard Methods for Vibration Testing of Shipping Containers," ASTM D 999, American Society for Testing and Materials, Philadelphia, PA, 1986.
2. Tappi, "Vibration Test for Fiberboard Shipping Containers," Official test method T817, 1984.
3. C.M. Harris, C.E. Crede, *Shock and Vibration Handbook*, 3d ed., McGraw-Hill, New York, 1988.
4. W.D. Godshall, "Frequency Response, Damping, and Transmissibility Characteristics of Top-Loaded Corrugated Containers," Res. Pap. FPL-160, Madison, WI: U.S. Department of Agriculture, Forest Service, Forest Products Laboratory, 1971.
5. W.D. Godshall, "Vibration Transmissibility Characteristics of Corrugated Fiberboard," Res. Pap. FPL-211. Madison, WI: U.S. Department of Agriculture, Forest Service, Forest Products Laboratory, 1973.
6. K. Peleg, "Frequency Response of Non-Linear Single Degree-of-Freedom Systems," *Int. J. Mech. Sci.*, Vol. 21, pp. 75-84, 1979.
7. K. Peleg, "Impact and Vibration Testing of Shipping Containers," *J. Sound and Vibration*, Vol. 93 No. 3, pp. 371-388, 1984.
8. T.J. Urbanik, "Vibrational Loading Mechanism of Unitized Corrugated Containers With Cushions and Non-Load-Bearing Contents," *Shock and Vibration Bull.*, No. 54, Pt. 3, pp. 111-121, 1984.
9. R.M. Phelan, *Dynamics of Machinery*, McGraw-Hill, New York, 1967.
10. J.R. Rice, *Numerical Methods, Software, and Analysis*, McGraw-Hill, New York, 1983.
11. T.J. Urbanik, "Force Plate for Corrugated Container Vibration Tests," *ASTM J. Test. Eval.*, Vol. 18, No. 5, pp. 359-362, 1990.
12. J.W. Mekee, J.W. Gander, and J.R. Wachuta, "Compression Strength Formula for Corrugated Boxes, *Paperboard Pkg.*, Aug. 1963.
13. P.E. Shick, N.C.S. Chari, "Top-to-Bottom Compression for Double Wall Corrugated Boxes," *Tappi*, Vol. 48, No. 7, pp. 423-430, 1965.